Solid-State Coordination Chemistry of Metal Oxides: Hydrothermal Synthesis and Structural Characterization of *o*-Phenanthroline-Ligated Copper− and Zinc−Molybdenum Oxides

Pamela J. Hagrman[†] and Jon Zubieta*

Department of Chemistry, Syracuse University, Syracuse, New York 13244

Received March 26, 1999

The hydrothermal chemistry of molybdate with phenanthroline in the presence of M(II) cations was investigated. With Cu(II) starting materials, modifications in reaction conditions yielded the molecular cluster [Cu(*o*-phen)$_2$Mo$_4$O$_{13}$] (**MOXI-27**) and one-dimensional [Cu(*o*-phen)MoO$_4$]·H$_2$O (**MOXI-28**). The analogous Zn(II)-containing one-dimensional material [Zn(*o*-phen)MoO$_4$] (**MOXI-29**) was isolated under conditions similar to those employed for the preparation of **MOXI-28**. Crystal data: $C_{24}H_{16}CuMo_4N_4O_{13}$ (**MOXI-27**), monoclinic, $P2_1/c$, $a = 10.5218(3)$ Å, $b = 12.1113(4)$ Å, $c = 22.0125(7)$ Å, $\beta = 97.988(1)°$, $Z = 4$; $C_{12}H_{10}CuMoN_2O_5$ (**MOXI-28**), monoclinic, $P2_1/n$, $a = 14.050(1)$ Å, $b = 5.8818(4)$ Å, $c = 16.227(1)$ Å, $\beta = 103.586(1)°$, $Z = 4$; $C_{12}H_8MoN_2O_4Zn$ (**MOXI-29**), monoclinic, $P2_1/m$, $a = 8.7714(7)$ Å, $b = 6.4172(2)$ Å, $c = 10.652(1)$ Å, $\beta = 100.702(5)°$, $Z = 2$.

Oxides are ubiquitous materials[1,2] with a range of physical properties that endow them with applications to catalysis, sorption, energy storage, molecular electronics, optical materials, and ceramics.[3,4] Although simple naturally occurring oxides can have unique and specific properties, such as piezoelectricity, ferromagnetism, or catalytic activity, as a general rule there is a correlation between the complexity of the structure of material and functionality.[5] One approach to the design of novel materials is the introduction of organic molecules to effect modification of the inorganic microstructure.[5] Such strategies mimic the natural process of biomineralization, where the inorganic component contributes to the increased functionality via assimilation as one component in a hierarchical structure in which there is a synergistic interaction between an organic and an inorganic component.[6,7] This interaction within such composite organic−inorganic materials must ultimately derive from the nature of the interface between the organic material and inorganic component. Synthetic studies of materials possessing such an interface, coupled with the acquisition of the appropriate structural information, should contribute to the development of an increased understanding of how to control the structure−property relationships within these composite materials.

Four primary classes of oxides in which organic materials play a significant structural role have been elaborated: zeolites,[8] mesoporous oxides of the MCM-41 type,[9] biomineralized materials, and microporous transition metal phosphates with entrained organic cations.[10] We have recently begun to develop a potential fifth class of such composite organic−inorganic materials: phases constructed from vanadium or molybdenum oxide substructures modified by organonitrogen ligands, identified as the **VOXI** and **MOXI** families.[11−18] An organic component of these composites may adopt a variety of structural roles. Organic substituents may be introduced as ligands covalently linked to the inorganic backbone of the solid. Such materials include the one-dimensional vanadium oxide phases [VO(VO$_3$)$_6${VO(2,2′-bpy)$_2$}$_2$][19] and [V^{IV}V$^{V}_2$O$_7$(phen)][20] and the three related one-dimensional molybdenum oxide phases [MoO$_3$(2,2′-bpy)], [Mo$_2$O$_6$(2,2′-bpy)], and [Mo$_3$O$_9$(2,2′-bpy)$_2$].[15] Another mode of attachment observed for these ligands is as "tethers" between metal sites, a modality commonly adopted by 4,4′-bipyridine as observed, for example, in [MoO$_3$(4,4′-bpy)$_{0.5}$].[21] Incorporation of complex transition metal/organic components into the covalent backbone of metal oxide solids, either as peripheral moieties or as complex bridging units, has

[†] Formerly Pamela J. Zapf.

(1) Wells, A. F. *Structural Inorganic Chemistry*, 4th ed.; Oxford University Press: Oxford, England, 1975.
(2) Greenwood, N. N.; Earnshaw, A. *Chemistry of the Elements*; Pergannon Press: New York, 1984.
(3) Cheetham, A. K. *Science* **1994**, *264*, 794 and references therein.
(4) Cox, P. A. *Transition Metal Oxides*; Clarendon Press: Oxford, England, 1995.
(5) Stupp, S. I.; Braun, P. V. *Science* **1997**, *277*, 1242.
(6) Hench, L. L. In *Materials Chemistry: An Emerging Discipline*; Interrante, L. V., Caspar, L. A., Ellis, A. B., Eds.; ACS Symposium Series 245; American Chemical Society: Washington, DC, 1995; Chapter 21, p 523.
(7) Mann, S. *Nature* **1993**, *365*, 499.
(8) (a) Smith, J. V. *Chem. Rev.* **1988**, *88*, 149. (b) Occelli, M. L.; Robson, H. C. *Zeolite Syntheses*; American Chemical Society: Washington, DC, 1989.
(9) Kresge, C. T.; Leonowicz, M. E.; Roth, W. J.; Vartuli, J. C.; Beck, J. S. *Nature* **1992**, *359*, 710.
(10) (a) Haushalter, R. C.; Mundi, L. A. *Chem. Mater.* **1992**, *4*, 31. (b) Khan, M. I.; Myer, L. M.; Haushalter, R. C.; Schweitzer, A. L.; Zubieta, J.; Dye, J. L. *Chem. Mater.* **1996**, *8*, 43.
(11) Zhang, Y.; DeBord, J. R. D.; O'Connor, C. J.; Haushalter, R. C.; Clearfield, A.; Zubieta, J. *Angew. Chem., Int. Ed. Engl.* **1996**, *35*, 989.
(12) DeBord, J. R. D.; Zhang, Y.; Haushalter, R. C.; Zubieta, J.; O'Connor, C. J. *J. Solid State Chem.* **1996**, *122*, 251.
(13) Hagrman, D.; Zubieta, C.; Rose, D. J.; Zubieta, J.; Haushalter, R. C. *Angew. Chem., Int. Ed. Engl.* **1997**, *36*, 873 and references therein.
(14) Zapf, P. J.; Haushalter, R. C.; Zubieta, J. *Chem. Commun.* **1997**, 321.
(15) Zapf, P. J.; Haushalter, R. C.; Zubieta, J. *Chem. Mater.* **1997**, *9*, 2019.
(16) Zapf, P. J.; Warren, C. J.; Haushalter, R. C.; Zubieta, J. *Chem. Commun.* **1997**, 1543.
(17) Zapf, P. J.; Hammond, R. P.; Haushalter, R. C.; Zubieta, J. *Chem. Mater.* **1998**, *10*, 1366.
(18) Hagrman, D.; Zapf, P. J.; Zubieta, J. *Chem. Commun.* **1998**, 1283.
(19) Huan, G.; Johnson, J. W.; Jacobson, A. J.; Merola, J. S. *J. Solid State Chem.* **1991**, *91*, 385.
(20) Duan, C.; Tian, Y; Lu, Z; You, X. *Inorg. Chem.* **1995**, *34*, 1.

10.1021/ic990340p CCC: $18.00
Published on Web 09/15/1999

Table 1. Crystal Data and Structure Refinement Summary for [Cu(*o*-phen)$_2$Mo$_4$O$_{13}$] (**MOXI-27**), [Cu(*o*-phen)MoO$_4$]·H$_2$O (**MOXI-28**), and [Zn(*o*-phen)MoO$_4$] (**MOXI-29**)[a]

	MOXI-27	MOXI-28	MOXI-29
empirical formula	$C_{24}H_{16}CuMo_4N_4O_{13}$	$C_{12}H_{10}CuMoN_2O_5$	$C_{12}H_8MoN_2O_4Zn$
fw	1015.71	421.70	405.51
space group	$P2_1/c$	$P2_1/n$	$P2_1/m$
temp, K	293(2)	293(2)	120(2)
a, Å	10.5218(3)	14.050(1)	8.7714(7)
b, Å	12.1113(4)	5.8818(4)	6.4172(2)
c, Å	22.0125(7)	16.227(1)	10.652(1)
β, deg	97.988(1)	103.586(1)	100.702(5)
V, Å^3	2777.9(2)	1303.5(2)	589.17(7)
Z	4	4	2
ρ_{calc}, Mg/m^3	2.429	2.149	2.286
μ, mm^{-1}	2.587	2.616	3.114
R1,[b] wR2[c] [$I > 2\sigma(I)$]	0.0622, 0.1484	0.0753, 0.1845	0.0190, 0.0479
R1,[b] wR2[c] (all data)	0.0950, 0.1617	0.1101, 0.2054	0.0209, 0.0485

[a] All data were collected on a Bruker SMART-CCD system using Mo Kα radiation (λ = 0.710 73 Å). [b] $R1 = \sum||F_o| - |F_c||/\sum|F_o|$. [c] $wR2 = [\sum[w(F_o^2 - F_c^2)^2]/\sum[w(F_o^2)^2]]^{1/2}$.

also been reported, including such vanadium oxide-based examples as [(2,2′-bpy)$_2$Zn]$_2$[V$_6$O$_{17}$][11] (**VOXI-1**) and the three related phases [Cu(H$_2$N(CH$_2$)$_2$NH$_2$)][V$_2$O$_6$], [Cu(2,2′-bpy)][V$_2$O$_6$], and [Cu(2,2′-bpy)$_2$][V$_2$O$_6$][12] (**VOXI 2−4**). Examples based on molybdenum oxides include one-dimensional [Ni(2,2′-bpy)$_2$Mo$_4$O$_{13}$] (**MOXI-10**) and [Cu(2,2′-bpy)Mo$_2$O$_7$] (**MOXI-17**) and two-dimensional [Co(2,2′-bpy)Mo$_3$O$_{10}$][14] (**MOXI-18**) and [{Ni(H$_2$O)$_2$(4,4′-bpy)$_2$}$_2$Mo$_8$O$_{26}$][13] (**MOXI-14**).

The structural diversity of such composite oxides derives from the interplay of a variety of factors. For the organic component, these include relative dispositions of donor groups, tether length, and steric influence of additional substituents. The presence of a secondary transition metal center and its coordination preferences and oxidation state are also determinants of structure for the mixed-metal oxides. Furthermore, reaction conditions of pH, temperature, and concentration of reactants may influence the product distribution.

As part of our continuing investigations of the organonitrogen−molybdenum oxide interface, the reactions of molybdenum oxides with *o*-phenanthroline in the presence of Cu(II) and Zn(II) were investigated. Under conditions similar to those employed for the 2,2′-bipyridine system, the molecular cluster [Cu(*o*-phen)$_2$Mo$_4$O$_{13}$] (**MOXI-27**) and the one-dimensional bimetallic oxides [Cu(*o*-phen)MoO$_4$]·H$_2$O (**MOXI-28**) and [Zn(*o*-phen)MoO$_4$] (**MOXI-29**) were isolated. Curiously, the structures of the one-dimensional phases are quite distinct from that observed previously for the bipyridine series [Cu(2,2′-bpy)Mo$_2$O$_7$] (**MOXI-17**). In this paper, the structures of **MOXI 27−29** are described and discussed in relation to other members of the **MOXI** family of materials.

Experimental Section

Reagents were purchased from Aldrich Chemical Co. and used without further purification. All syntheses were carried out in 23 mL poly(tetrafluoroethylene)-lined stainless steel containers under autogenous pressure. The reactants were stirred briefly before heating. All distilled water used was distilled above 3.0 Ω in-house using a Barnstead model 525 Biopure Distilled Water Center.

Synthesis of [Cu(*o*-phen)$_2$Mo$_4$O$_{13}$] (MOXI-27). A mixture of MoO$_3$ (0.0649 g, 0.45 mmol), *o*-phenanthroline (0.0812 g, 0.45 mmol), CuSO$_4$·5H$_2$O (0.0549 g, 0.22 mmol), and H$_2$O (8.076 g, 448 mmol) was heated at 180 °C for 68 h. After 3 h of cooling, dark green blocks of **MOXI-27** were collected in 45% yield.

Synthesis of [Cu(*o*-phen) MoO$_4$]·H$_2$O (MOXI-28). A mixture of Na$_2$MoO$_4$·2H$_2$O (0.217 g, 0.90 mmol), *o*-phenanthroline (0.162 g, 0.90 mmol), CuCl$_2$·2H$_2$O (0.154 g, 0.90 mmol), and H$_2$O (8.046 g, 447 mmol) in the mole ratio 1:1:1:500 was heated at 160 °C for 3 d. After 3 h of cooling blue plates of **MOXI-28** were collected in 15% yield by mechanical separation from white amorphous material.

Synthesis of [Zn(*o*-phen) MoO$_4$] (MOXI-29). The pH of a mixture of Na$_2$MoO$_4$·2H$_2$O (0.056 g, 0.23 mmol), *o*-phenanthroline (0.040 g, 0.22 mmol), ZnCl$_2$ (0.031 g, 0.23 mmol), and H$_2$O (8.0261 g, 446 mmol) in the mole ratio 1:1:1:1940 was adjusted by the addition of 0.1 mL of (C$_2$H$_5$)$_4$NOH (20% in H$_2$O, 0.1 mL) to ca. pH 6. After the mixture was heated at 165 °C for 24 h, colorless blocks of **MOXI-29** were collected in 45% yield.

X-ray Crystallography. Structural measurements for **MOXI-27−29** were performed on a Bruker SMART-CCD diffractometer at a temperature of 150 ± 1 K using graphite-monochromated Mo *K*α radiation (λ(Mo *K*α) = 0.710 73 Å).

The data were corrected for Lorentz and polarization effects. The structures were solved by direct methods.[22] In all cases, all non-hydrogen atoms were refined anisotropically. Neutral-atom scattering factors were taken from Cromer and Waber,[23] and anomalous dispersion corrections were taken from Creagh and McAuley.[24] All calculations were performed using the SHELXTL[25] crystallographic software packages.

Crystallographic details for the structures of **MOXI-27−29** are summarized in Table 1. Atomic positional parameters, full tables of bond lengths and angles, and anisotropic temperature factors are available in the Supporting Information. Selected bond lengths and angles for **MOXI-27−29** are given in Tables 2−4, respectively. The atom-labeling schemes and thermal ellipsoids for **MOXI-27−29** are shown in Figure 6.

Results and Discussion

The isolation of **MOXI-27−29** relies on hydrothermal techniques.[26,27] By the employment of temperatures in the 120−250 °C range under autogenous pressures, rather than the high-temperature methods more routinely used in solid-state chemistry, "self-assembly" of metastable phases that retain the bond relationships between most of the consituent atoms may be

(21) (a) Johnson, J. W.; Jacobson, A. J.; Rich, S. M.; Brody, J. F. *J. Am. Chem. Soc.* **1981**, *103*, 5346. (b) Zapf, P. J.; LaDuca, R. L.; Warren, C. J.; Zubieta, J. Unpublished results.

(22) *SHELXTL*; PC Siemens Analytical X-ray Instruments: Madison WI, 1993.

(23) Cromer, D. T.; Waber, J. T. *International Tables for X-ray Crystallography*; Kynoch Press: Birmingham, England, 1974; Vol. IV.

(24) Creagh, D. C.; McAuley, J. W. J. *International Tables for X-ray Crystallography*; Kluwer Academic: Boston, MA, 1992; Vol. C, Table 4.2.6.8.

(25) Sheldrick, G. M. *SHELXTL Structure Determination Programs*, Version 5.0; PC Siemens Analytical Systems: Madison, WI, 1994.

(26) Khan, I.; Zubieta, J. *Prog. Inorg. Chem.* **1995**, *43*, 1.

(27) Fuchs, J.; Hartl, H. *Angew. Chem., Int. Ed. Engl.* **1977**, *16*, 952.

Table 2. Selected Bond Lengths (Å) and Angles (deg) for $[Cu(o\text{-phen})_2Mo_4O_{13}]$ (**MOXI-27**)[a]

Mo(1)−O(2)	1.689(6)	Mo(3)−O(7)	1.934(5)
Mo(1)−O(1)	1.719(5)	Mo(3)−O(10)	2.354(5)
Mo(1)−O(7)#1	1.892(5)	Mo(3)−O(6)	2.376(6)
Mo(1)−O(4)	1.909(5)	Mo(4)−O(12)	1.691(6)
Mo(1)−O(6)#1	2.396(5)	Mo(4)−O(13)	1.706(5)
Mo(1)−O(3)	2.443(5)	Mo(4)−O(11)	1.896(5)
Mo(2)−O(5)	1.690(5)	Mo(4)−O(4)	1.901(5)
Mo(2)−O(10)#1	1.778(5)	Mo(4)−O(10)	2.423(5)
Mo(2)−O(6)	1.788(5)	Cu(5)−N(3)	1.969(6)
Mo(2)−O(3)	1.791(6)	Cu(5)−N(1)	1.979(6)
Mo(3)−O(9)	1.686(6)	Cu(5)−N(4)	2.059(6)
Mo(3)−O(8)	1.691(5)	Cu(5)−N(2)	2.101(6)
Mo(3)−O(11)	1.926(5)	Cu(5)−O(1)	2.192(5)
N(3)−Cu(5)−N(1)	176.3(3)	N(4)−Cu(5)−N(2)	136.2(3)
N(3)−Cu(5)−N(4)	81.9(3)	N(3)−Cu(5)−O(1)	90.3(2)
N(1)−Cu(5)−N(4)	98.1(2)	N(1)−Cu(5)−O(1)	86.8(2)
N(3)−Cu(5)−N(2)	100.5(3)	N(4)−Cu(5)−O(1)	128.9(2)
N(1)−Cu(5)−N(2)	82.1(2)	N(2)−Cu(5)−O(1)	94.9(2)

[a] Symmetry transformation used to generate equivalent atoms: (#1) $-x, -y, -z$.

Table 3. Selected Bond Lengths (Å) and Angles (deg) for $[Cu(o\text{-phen})MoO_4]\cdot H_2O$ (**MOXI-28**)[a]

Mo(1)−O(1)	1.733(6)	Cu(2)−O(2)#2	1.930(6)
Mo(1)−O(2)	1.762(6)	Cu(2)−N(2)	2.010(7)
Mo(1)−O(4)	1.764(5)	Cu(2)−N(1)	2.043(6)
Mo(1)−O(3)	1.784(5)	Cu(2)−O(4)	2.259(5)
Cu(2)−O(3)#1	1.929(5)		
O(1)−Mo(1)−O(2)	110.1(3)	O(3)#1−Cu(2)−O(2)#2	93.2(2)
O(1)−Mo(1)−O(4)	107.4(3)	O(3)#1−Cu(2)−N(2)	90.0(2)
O(2)−Mo(1)−O(4)	109.8(2)	O(2)#2−Cu(2)−N(2)	170.7(3)
O(1)−Mo(1)−O(3)	109.0(3)	O(3)#1−Cu(2)−N(1)	167.0(3)
O(2)−Mo(1)−O(3)	111.0(3)	O(2)#2−Cu(2)−N(1)	93.7(2)
O(4)−Mo(1)−O(3)	109.5(3)		

[a] Symmetry transformations used to generate equivalent atoms: (#1) $x, y + 1, z$; (#2) $-x + 1, -y + 1, -z + 1$; (#3) $x, y - 1, z$.

Table 4. Selected Bond Lengths (Å) and Angles (deg) for $[Zn(o\text{-phen})MoO_4]$ (**MOXI-29**)[a]

Mo(1)−O(2)	1.720(2)	Zn(2)−O(1)#3	1.9899(13)
Mo(1)−O(3)	1.756(2)	Zn(2)−O(3)	2.025(2)
Mo(1)−O(1)#1	1.7832(13)	Zn(2)−N(1)	2.108(2)
Mo(1)−O(1)	1.7832(13)	Zn(2)−N(2)	2.151(2)
Zn(2)−O(1)#2	1.9899(13)		
O(2)−Mo(1)−O(3)	108.41(10)	O(1)#3−Zn(2)−O(3)	93.38(5)
O(2)−Mo(1)−O(1)#1	109.11(6)	O(1)#2−Zn(2)−N(1)	117.76(4)
O(3)−Mo(1)−O(1)#1	110.34(6)	O(1)#3−Zn(2)−N(1)	117.76(4)
O(2)−Mo(1)−O(1)	109.11(6)	O(3)−Zn(2)−N(1)	93.40(9)
O(3)−Mo(1)−O(1)	110.34(6)	O(1)#2−Zn(2)−N(2)	90.49(5)
O(1)#1−Mo(1)−O(1)	109.51(9)	O(1)#3−Zn(2)−N(2)	90.49(5)
O(1)#2−Zn(2)−O(1)#3	123.43(8)	O(3)−Zn(2)−N(2)	171.82(8)
O(1)#2−Zn(2)−O(3)	93.38(5)		

[a] Symmetry transformations used to generate equivalent atoms: (#1) $x, -y + 1/2, z$; (#2) $-x + 1, -y, -z$; (#3) $-x + 1, y + 1/2, -z$.

accomplished from simple molecular precursors. The reduced viscosity of water under these conditions promotes solvent extraction of solids and crystal growth from solution. More specifically, differential solubilities of organic and inorganic components in the medium are minimized, allowing the introduction of a variety of organic or complex metal−ligand components into the reaction mixture. However, since the method of synthesis depends on self-assembly of the products from the molecular precursors, the elements of mechanistic control are generally absent and the identity of the products under a given set of conditions is often unpredictable. On the other hand, the accessibility of a vast parameter space, including

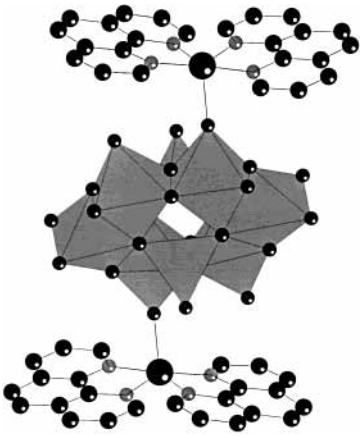

Figure 1. View of the structure of **MOXI-27**. The α-$[Mo_8O_{26}]^{4-}$ cluster is shown as a polyhedral representation while the $[Cu(o\text{-phen})_2]$ portion is illustrated using a ball-and-stick representation.

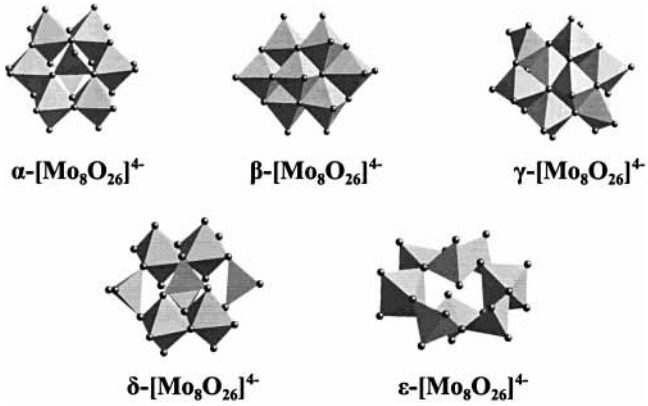

Figure 2. The five octamolybdate isomers as polyhedral representations.

stoichiometries, temperature, pressure, pH, fill volume, starting materials, templates, and mineralizers, permits significant variations in conditions for the isolation of both molecular species and solid-phase materials for similar compositional systems, as previously noted for the oxovanadium−organophosphonate class of compounds.[26] Faux de mieux, the reaction domain must be explored in the absence of a well-developed mechanistic understanding. However, the judicious manipulation of reaction conditions can provide reliable conditions for the isolation of novel materials.

These general considerations have guided the synthesis of **MOXI-27**−**29**. Thus, the hydrothermal reaction of MoO_3, *o*-phenanthroline, and $CuSO_4\cdot 5H_2O$ in water at 180 °C for 68 h yielded the molecular cluster $[Cu(o\text{-phen})_2Mo_4O_{13}]$ **(MOXI-27)** as dark green crystals in good yield. In contrast, when MoO_3 and $CuSO_4\cdot 5H_2O$ are replaced by $Na_2MoO_4\cdot 2H_2O$ and $CuCl_2\cdot 2H_2O$ and the temperature is reduced to 160 °C, the one-dimensional phase $[Cu(o\text{-phen})MoO_4]\cdot H_2O$ **(MOXI-28)** is isolated. The conditions for the isolation of **MOXI-28** appear to be quite critical, and the material is isolable only in a narrow region of the reaction domain. At 160 °C, substitution of MoO_3 for $Na_2MoO_4\cdot 2H_2O$ or of $CuSO_4\cdot 5H_2O$ for $CuCl_2\cdot 2H_2O$ yields amorphous mixtures. Likewise, **MOXI-28** forms from MoO_3 and $CuCl_2\cdot 2H_2O$ only in the 140−160 °C temperature range.

Attempts to isolate the Zn(II) analogue of **MOXI-28** required the adjustment of the initial reaction pH to ca. 6. Thus, the reaction of $Na_2MoO_6\cdot 2H_2O$, *o*-phenanthroline, and $ZnCl_2$ in water at 160 °C for 24 h produced colorless blocks of $[Zn(o\text{-phen})MoO_4]$ (**MOXI-29**) in good yield.

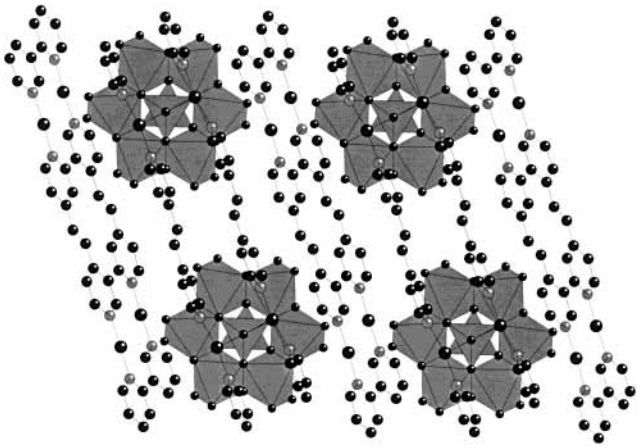

Figure 3. Structure of $[\{Cu(4,4'\text{-bipyridyl-1,2-ethene})\}_4Mo_8O_{26}]$ showing the α-$[Mo_8O_{26}]^{4-}$ clusters linked through $\{Cu(bpe)\}_n^{n+}$ chains.

As shown in Figure 1, the structure of **MOXI-27** consists of discrete $[\{Cu(o\text{-phen})_2\}_2M_8O_{26}]$ clusters, constructed from α-octamolybdate clusters linked to two $\{Cu(o\text{-phen})_2\}^{2+}$ groups. The $\{Mo_8O_{26}\}^{4-}$ moiety exhibits the characteristic α-octamolybdate arrangement of six edge-sharing molybdenum octahedra forming an equatorial girdle with a tetrahedral η^3-μ_6-$\{MoO_4\}^{2-}$ group occupying either pole.

Each $\{Cu(o\text{-phen})_2\}^{2+}$ group bonds to a single terminal oxoligand of an octahedral molybdenum site. These copper coordination complex subunits are bonded to two transannular molybdenum sites and disposed above and below the mean plane of the eight molybdenum centers. Thus, the copper sites exhibit distorted square pyramidal $\{CuN_4O\}$ geometry.

The structure of the octamolybdate core of **MOXI-27** is unperturbed with respect to that of the parent $\{\alpha\text{-}Mo_8O_{26}\}^{4-}$ cluster, with the exception of a small lengthening of the Mo−O bond to the oxo ligand employed in bridging to the copper unit. Thus, while the average value for all other Mo−terminal oxo ligand bond lengths for the octahedral sites of **MOXI-27** is 1.693(7) Å, the Mo−O bond length for the bridging oxo ligand is 1.719(5) Å.[27]

The occurrence of polyoxoanions supporting organometallic fragments [28−41] or transition metal coordination complexes[42,43] as convalently bound subunits of the metal oxide substructure is not unusual. In fact, octamolybdate substructures decorated with transition metal coordination complex appendages are common structural motifs in the hydrothermal chemistry of these phases. As shown in Figure 2, five octamolybdate isomers have been identified. While the α, β, γ,and δ forms exist as isolated anion clusters,[44,45] the ϵ form has been identified only as a substructure of a more complex solid-state assembly.[13] The α-molybdate cluster has also been identified as a component of the three-dimensional structure of $[\{Cu(4,4'\text{-bipyridyl-1,2-ethene})\}_4Mo_8O_{26}]$.[46] However, in this instance, as shown in Figure 3, the polymeric coordination complex cation component $\{Cu(bpe)\}_n^{n+}$ links to the $[Mo_8O_{26}]^{4-}$ cluster through the apical oxo ligands of the polar-capping tetrahedral molybdate units. The oxo ligands serve to bridge the cluster to two parallel cationic strands to form a $[\{Cu(bpe)\}_2Mo_8O_{26}]^{2-}$ layer. The contrasting structures of **MOXI-27** and $[\{Cu(bpe)\}_4Mo_8O_{26}]$

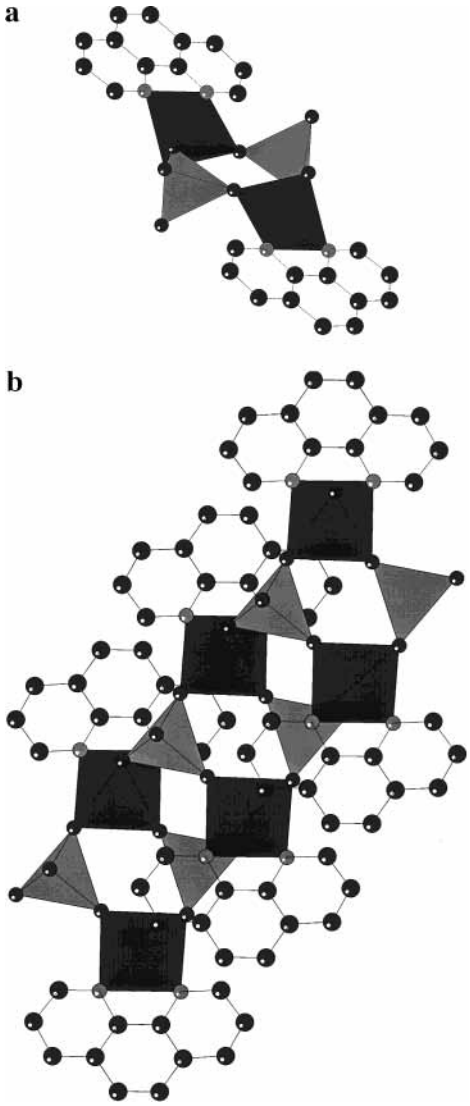

Figure 4. Structure of **MOXI-28** (a) viewed down the chain axis which propagates parallel to the crystallographic *b* axis and (b) viewed normal to the plane of the *o*-phenanthroline ligands. Copper square pyramids are shown as darker shaded polyhedra, while the molybdenum tetrahedra are shown with lighter shading.

(28) Day, V. W.; Klemperer, W. G. In *Polyoxometalates: From Platonic Solids to Antiretroviral Activity*; Pope, M. T., Müller, A., Eds.; Kluwer Academic Press: Dordrecht, The Netherlands, 1994; p 87.
(29) Day, V. W.; Klemperer, W. G.; Yagaseki, A. *Chem. Lett.* **1990**, 1267.
(30) Besecher, C. J.; Day, V. W.; Klemperer, W. G.; Thompson, M. R. *Inorg. Chem.* **1985**, *24*, 44.
(31) Chee, H. K.; Klemperer, W. G. *Inorg. Chem.* **1989**, *28*, 1424.
(32) Hayaski, Y.; Ozawa, Y.; Isobe, K. *Inorg. Chem.* **1991**, *30*, 1025.
(33) Day. V. W.; Klemperer, W. G.; Maine, D. J. *Inorg. Chem.* **1990**, *29*, 2345.
(34) Chae, H. K.; Klemperer, W. G.; Paez Loyo, D. E.; Day, V. W.; Eberspacher, T. A. *Inorg. Chem.* **1992**, *31*, 3187.
(35) Pohl, M.; Lyon, D. K.; Miguno, N.; Nomiza, K.; Finke, R. G. *Inorg. Chem.* **1995**, *34*, 1413.
(36) Nayko, B. M.; Pohl, M.; Finke, R. G. *Inorg. Chem.* **1994**, *33*, 3625.
(37) Weiner, H.; Aiken, J. D., III; Finke, R. G. *Inorg. Chem.* **1996**, *35*, 7905.
(38) Nagata, T.; Pohl, M.; Weiner, H.; Finke, R. G. *Inorg. Chem.* **1997**, *36*, 1366.
(39) Hayaski, Y.; Muller, F.; Lin, Y.; Miller, S. M.; Anderson, O. P.; Finke, R. G. *J. Am. Chem. Soc.* **1997**, *119*, 11401.
(40) Tokara, S.; Nishioha, T.; Kimoshita, I.; Isobe, K. *Chem. Commun.* **1997**, 891.
(41) Süss-Fink, G.; Plasseraud, L.; Ferrand, V.; Stoeckli-Evans, H. *Chem. Commun.* **1997**, 1657.
(42) DeBord, J. R. D.; Haushalter, R. C.; Meyer, L. M.; Rose, D. J.; Zapf, P. J.; Zubieta, J. *Inorg. Chim. Acta* **1997**, *256*, 165.
(43) Zhang, Y.; Zapf, P. J.; Meyer, L. M.; Haushalter, R. C.; Zubieta, J. *Inorg. Chem.* **1997**, *36*, 2159.
(44) Inone, M.; Yamasi, T. *Bull. Chem. Soc. Jpn.* **1995**, *68*, 3055 and references therein.
(45) Payne, M. T. *Prog. Inorg. Chem.* **1991**, *39*, 255.
(46) Stein, A. J.; Keller, S. W.; Mallouk, T. E. *Science* **1993**, *259*, 1558.

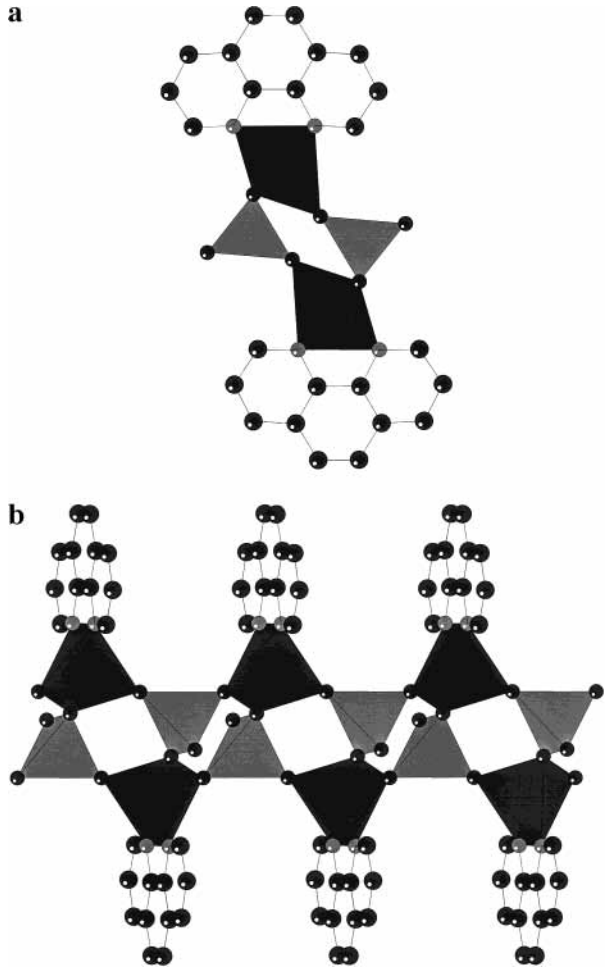

Figure 5. The one-dimensional chain of **MOXI-29** (a) viewed down the *b* axis and (b) emphasizing the connectivity and geometry of the zinc centers. Zinc polyhedra are shown with darker shading, while molybdenum tetrahedra have lighter shading.

serve to illustrate the often dramatic influences of ligand type and metal oxidation state and consequently coordination preferences on the overall architecture of materials constructed from metal oxide and coordination complex substructures. The β, γ, δ, and ϵ forms of the octamolybdate cluster contribute subunits to the structures of $[\{Cu_3(4,7\text{-phen})_3\}_2Mo_{14}O_{45}]$,[18] $[\{Cu(en)_2\}_2Mo_8O_{26}]$,[42] $[\{Cu(4,4'\text{-bpy})\}_4Mo_8O_{26}]$,[13] and $[\{Ni(4,4'\text{-bpy})_2(H_2O)_2\}_2Mo_8O_{26}]$,[13] respectively. The β-molybdate type is also a motif of the one-dimensional chain structure of $[\{Ni(2,2'\text{-bpy})_2\}_2Mo_8O_{26}]$.[16]

In contrast to the molecular structure of **MOXI-27**, the structure of [Cu(*o*-phen)MoO_4] **(MOXI-28)**, shown in Figure 4, consists of one-dimensional chains constructed from $\{MoO_4\}$ tetrahedra bridging square pyramidal $\{Cu(o\text{-phen})O_3\}$ subunits in a corner-sharing arrangement of polyhedra. Each $\{MoO_4\}^{2-}$ unit adopts an η^3,μ_3-coordination mode, bridging three adjacent $\{CuN_2O_3\}$ polyhedra. The structure may be described in terms of $\{Mo_2Cu_2O_4\}$ rings fused into a puckered one-dimensional ribbon. As a consequence of the square pyramidal geometry at the Cu centers, the *o*-phenanthroline rings are tilted with respect to the direction of propagation of the $\{Cu_2Mo_2O_4\}$ chain at an angle of 122.7°.

Substitution of Zn(II) for Cu(II) results in the analogous structure of [Zn(*o*-phen)MoO_4] **(MOXI-29)**. As shown in Figure 5, the structure of **MOXI-29** contrasts with that of **MOXI-28** with respect to the coordination environment of the M(II) site. While the Cu site of **MOXI-28** is distinctly square pyramidal,

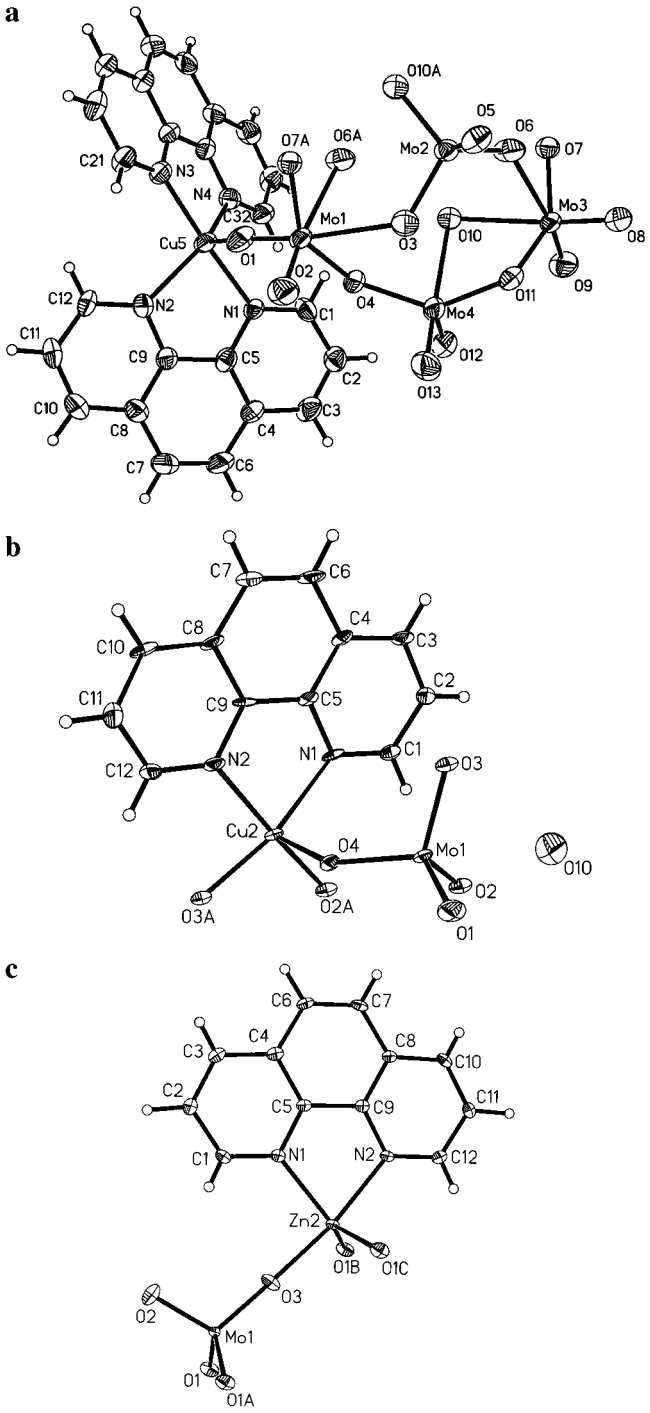

Figure 6. Atom-labeling schemes and thermal ellipsoid plots (50% probability) for (a) **MOXI-27**, (b) **MOXI-28**, and (c) **MOXI-29**.

the Zn(II) center of **MOXI-29** enjoys trigonal bipyramidal geometry (Table 4). The major structural consequence is the disposition of the *o*-phen plane with respect to the $\{Cu_2Mo_2O_4\}$ chain. As shown in Figure 5, the ring plane is normal to the chain axis, rather than tilted as for **MOXI-28**.

The structures of **MOXI-28** and **MOXI-29** are reminiscent of that of [Fe(2,2′-bpy)ClMoO_4] **(MOXI-21)**. The structure of the Fe(III) derivative is likewise constructed from fused $\{Fe_2Mo_2O_4\}$ rings. However, the polyhedral motifs consist of $\{MoO_4\}$ tetrahedra and $\{FeN_2O_3Cl\}$ octahedra, rather than the five-coordinate trigonal bipyramidal or square pyramidal substructures associated with **MOXI-28** and **MOXI-29**.

The contrasting structures of the one-dimensional chains of **MOXI-21**, **MOXI-28**, and **MOXI-29** reveal the structure-

determining role of the coordination preferences of the secondary metal site. Thus, the tendency of Cu(II) to form tetragonally distorted "4+1" or "4+2" sites is reflected in the tilting of *o*-phenanthroline rings of **MOXI-28**, which is a consequence of the square pyramidal geometry. The coordination polyhedron flexibility of the d^{10} Zn(II) center is manifest in the trigonal bipyramidal geometry of **MOXI-29**, while the preference of Fe(III) for octahedral coordination and the requirements of charge compensation result in the $\{FeN_2O_3Cl\}$ coordination of **MOXI-21**.

Conclusions

The isolation of **MOXI-28** and **MOXI-29** reinforces the observation that numerous metastable oxometalate solid phases may be prepared by hydrothermal techniques.[46] Furthermore, the isolation of **MOXI-27** demonstrates that there are domains in the hydrothermal parameter space which favor the isolation of molecular species of unusual structures and nuclearities. The covalent attachment of the coordination complex fragment $\{Cu(o\text{-phen})_2\}^+$ to a polyoxomolybdate unit in **MOXI-27** suggests that a building block approach to solid oxide phases using discrete molecular species may be feasible. Indeed, the linking of polyoxomolybdate clusters through coordination complex units has been realized in one-dimensional $[Ni(2,2'\text{-bpy})_2Mo_4O_{13}]$[16] and in two-dimensional $[\{Cu_3(4,7\text{-phen})_3\}_2M_{14}O_{45}]$.[18]

The profound influences of organic components on oxide microstructures are also apparent in the structures of **MOXI 27**−**29**. The organic component in its role as a ligand on a secondary metal site serves to passivate the surface of the growing metal oxide substructure, consequently restricting the ability of the oxide to assume spatial extension in more than one dimension. The one-dimensional structures of **MOXI-28** and **MOXI-29** may be compared to that of $[FeCl(2,2'\text{-bpy})MoO_4]$,[17] which exhibits a similar bimetallic oxide core of alternating $\{MoO_4\}$ tetrahedral and $\{FeO_3ClN_2\}$ polyhedra. However, the influences of the coordination preferences of the secondary M(II)/M(III) site and of the ligand type also exert a structure-directing role. This is evident in the distinctive structures of $[Ni(2,2'\text{-bpy})_2Mo_4O_{13}]$, $[Cu(2,2'\text{-bpy})Mo_2O_7]$, and $[Co(2,2'\text{-bpy})Mo_3O_{10}]$,[16] which exhibit architectures significantly different from those of **MOXI-28** and **MOXI-29**. The application of principles derived from the coordination chemistry of classical complexes for the synthesis of solid phases provides a low-temperature approach to the development of new materials whose properties may be modified by judicious choices of subunits. However, the very complexity of the reaction domain and of the organic−inorganic interface has thus far rendered predictability an elusive goal.

Acknowledgment. This work was supported by NSF Grant CHE 9617232.

Supporting Information Available: X-ray crystallographic files, in CIF format, for **MOXI-27**−**29**. This material is available free of charge via the Internet at http://pubs.acs.org.

IC990340P